ACS Photonics

Letter

Cite This: ACS Photonics 2019, 6, 302−307

pubs.acs.org/journal/apchd5

Optical Control of Plasmonic Hot Carriers in Graphene

M. Mehdi Jadidi,[*,†,‡] Kevin M. Daniels,[†] Rachael L. Myers-Ward,[§] D. Kurt Gaskill,[§] Jacob C. König-Otto,[∥] Stephan Winnerl,[∥] Andrei B. Sushkov,[⊥] H. Dennis Drew,[⊥] Thomas E. Murphy,[†] and Martin Mittendorff[†,#]

[†]Institute for Research in Electronics and Applied Physics, University of Maryland, College Park, Maryland 20740, United States

[‡]Department of Applied Physics and Applied Mathematics, Columbia University, New York, New York 10027, United States

[§]U.S. Naval Research Laboratory, Washington, D.C. 20375, United States

[∥]Helmholtz-Zentrum Dresden-Rossendorf, P.O. Box 510119, 01314 Dresden, Germany

[⊥]Center for Nanophysics and Advanced Materials, University of Maryland, College Park, Maryland 20742, United States

[#]Fakultät für Physik, Universität Duisburg-Essen, 47057 Duisburg, Germany

ABSTRACT: Plasmons in subwavelength-structured graphene surfaces exhibit strong light−matter interaction and prominent resonance effects in the terahertz/mid-IR frequency range. Due to its exceptionally small electronic specific heat, graphene shows strong photoinduced hot electron effects that significantly alter the plasmon response. This can enable fast control of plasmon resonance through transient heating of carriers. We employ nonlinear pump−probe measurements on subwavelength graphene ribbons to explore the effect of photoinduced hot carriers on graphene plasmons. Measurements taken above and below the plasmon resonance frequency clearly demonstrate an optically induced red-shift of the plasmon resonance, which is a signature of hot carriers in the graphene. The observed photoinduced change in plasmon resonance exhibits very strong (of order 10%) and fast response times (few picoseconds), which are governed by the cooling rate of hot electrons. The results presented here contribute to the understanding of plasmonic hot carriers in graphene and can find applications in fast terahertz modulation and switching.

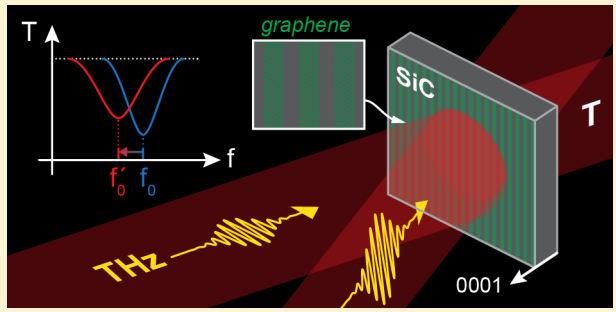

KEYWORDS: *graphene, nonlinear, plasmons, pump−probe, terahertz*

Graphene has been widely studied as an atomically thin nonlinear material that can be added or incorporated into other active or passive optical devices. In the visible and near-infrared regime, the linear and nonlinear optical properties of graphene are governed by the interband response, which is extremely broadband because of graphene's gapless, Dirac dispersion relation. Several nonlinear effects have been observed in graphene, including saturable absorption from Pauli blocking,[1−3] third-harmonic generation,[4,5] and four-wave mixing,[6,7] although in many cases the cumulative nonlinear efficiency is severely limited by the monolayer film thickness. Indeed, the first and most prevalent application of graphene as a nonlinear material remains as a saturable absorber in mode-locked lasers, an application that requires only a small fractional change in absorption.[8,9] In the terahertz spectral regime, by contrast, the conductivity of graphene is governed by intraband absorption, which is well-described by the Drude model. Graphene's unusual thermal properties, including small electron heat capacity and weak electron−phonon coupling, mean that the electrons responsible for the Drude absorption can be efficiently heated, thereby producing a hot-carrier nonlinearity that is absent or weak in conventional materials.[10−13] As the hot carriers in graphene cool down on a picosecond time scale, this nonlinearity can even be exploited for efficient harmonic generation in the THz regime.[14]

The light−matter interaction in many materials can be tuned and controlled by introducing plasmonic structures,[15] which also results in an increased nonlinear response.[16] When graphene is patterned into micron-scale ribbons, the electrons can collectively oscillate at a resonant frequency that depends on both the dimensions and the carrier concentration. These plasmon resonances can be tailored by lithographic patterning or electrically tuned throughout the terahertz regime.[17,18] When these graphene ribbons are illuminated at the resonant frequency, there is a significant increase in the absorption, which is accompanied by a dramatic electric field enhancement in the immediate vicinity of the ribbons.[17−22] Both effects can lead to an increase in the hot-carrier nonlinear interaction.[23] A very recent theoretical study by Cox and Abajo[24] confirms that hot carrier effects dominate the nonlinearity in graphene plasmons.

Received: October 29, 2018
Published: January 9, 2019

DOI: 10.1021/acsphotonics.8b01499
ACS Photonics 2019, 6, 302−307

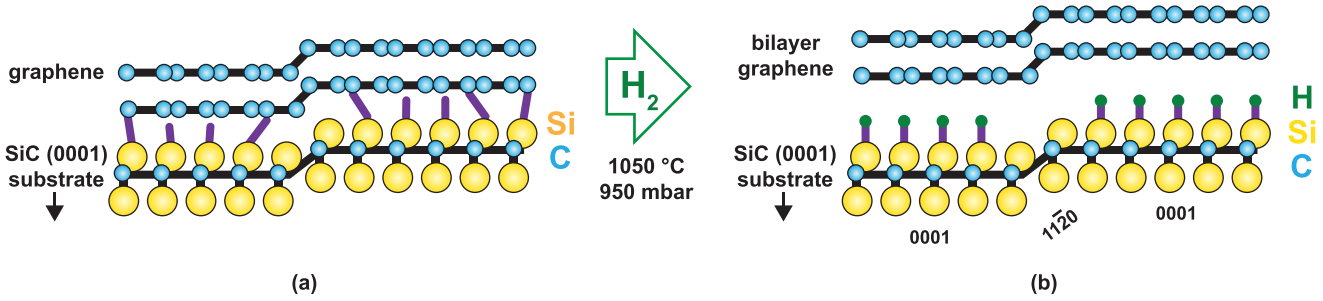

Figure 1. (a) Diagram of monolayer epitaxial graphene synthesized by the sublimation of silicon from the (0001) surface of SiC, prior to hydrogen intercalation. (b) After hydrogen intercalation, the Si dangling bonds of SiC are passivated with hydrogen and the buffer layer is promoted, forming quasi-freestanding bilayer graphene (QFS BLG) with significantly higher mobility and plasmon lifetime. Hydrogen intercalation only affects the terraces (0001) due to a lack of Si dangling bonds on the $(11\bar{2}0)$ steps of SiC.

In this study, we pattern graphene ribbons from quasi-freestanding epitaxial bilayer graphene that is produced by thermal decomposition of silicon carbide and hydrogen intercalation.[25,26] This process yields wafer-scale graphene with simultaneously high carrier mobility and concentration—conditions that are ideal for producing a sharp, strong plasmonic resonance.[27] The samples were measured using narrow band THz pulses from a free-electron laser, which were tuned across the plasmon resonance in order to probe the nature of the enhanced nonlinear response. Our measurements reveal a short-lived (~9 ps) and strong (~10%) pump-induced increase in transmission, which is about 10× stronger than previous results on patterned graphene grown by chemical vapor deposition. Measurements above and below resonance show clear evidence of a dynamical redshift of the plasmon frequency, validating a recent theoretical study based on hot carriers.[24]

1. FABRICATION

The epitaxial graphene used in these experiments was synthesized by sublimation of silicon from a ≈1 cm^{-2} coupon cut from a 6H-silicon carbide (SiC) wafer (II–VI, Inc.) and subsequent graphitization of carbon, resulting in the structure depicted in Figure 1a. Unlike conventional exfoliated or CVD-grown graphene, this process produces large area wafer-scale graphene films with high electrical and morphological uniformity needed for these experiments.[28] The reconstructed carbon buffer layer, which is bound to the SiC, increases the electron–phonon coupling and thereby limits the mobility due to the increased scattering rate of as-grown graphene.[26,29−31] Using a process of high-temperature hydrogen intercalation, the Si dangling bonds of the SiC are passivated with hydrogen, as shown in Figure 1b, which decouples the buffer layer from the SiC by converting it into a second layer under the first layer of graphene. The resulting combination is Bernal stacked. This quasi-freestanding bilayer epitaxial graphene shows a 4-fold increase in carrier mobility and a corresponding narrowing of the plasmon linewidth.[27]

The red curve in Figure 2 shows the transmission spectrum of the unpatterned bilayer graphene, which was measured using Fourier transform infrared spectroscopy (FTIR) and normalized relative to that of a bare SiC substrate. The superposed dashed line in Figure 2 shows the calculated transmission spectrum obtained from the Drude model, from which we estimate the carrier density and mobility to be n = 9.0×10^{12} cm^{-2} and μ_c = 3600 $cm^2\ V^{-1}\ s^{-1}$, respectively. These values are in substantial agreement with electrical Hall

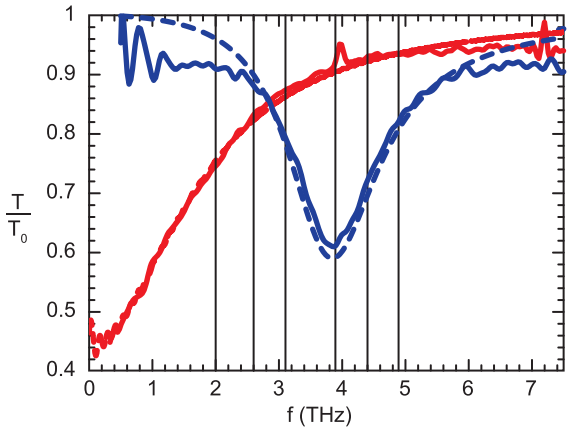

Figure 2. Measured (solid) and simulated (dashed) transmission spectrum of unpatterned graphene (red) and patterned graphene ribbons (blue). The vertical lines indicate the five THz frequencies above and below resonance at which nonlinear response of the sample was measured: 2.0, 2.5, 3.1, 3.9, 4.4, and 4.9 THz.

measurements performed on samples prepared similarly to those in this work.[27]

The graphene was patterned via electron-beam lithography and subsequent oxygen plasma etching to produce ribbons with width w = 900 nm and a periodicity of Λ = 1200 nm. The blue curve in Figure 2 is the measured THz transmission spectrum of the ribbons, which shows strong (35%) extinction at the plasmon resonant frequency of 3.9 THz when the illumination is polarized perpendicular to the ribbons. The transmission spectrum of the graphene ribbons can be modeled using the Drude-Lorentz model,[23] which predicts a Lorentzian dip in transmission centered at the plasmon frequency, indicated by the blue dashed line. The transmission spectrum of the graphene ribbons was calculated using the previously determined mobility and carrier concentration, the plasmon frequency served as a free parameter in the Drude-Lorentz formula.

2. NONLINEAR MEASUREMENT

The nonlinear response of the graphene sample was measured using a free-electron laser (FELBE facility, located at Helmholtz-Zentrum Dresden-Rossendorf), which produces high-power pulses with a repetition rate of 13 MHz that can be freely tuned throughout the THz range. Importantly, the spectral width of the FEL source in our experiments was approximately 30 GHz, which is much smaller than the

DOI: 10.1021/acsphotonics.8b01499
ACS Photonics 2019, 6, 302−307

plasmon linewidth shown in Figure 2. In contrast to the narrow-band pulses of the FEL, table-top sources based on optical rectification of femtosecond pulses or photoconductive emission deliver multioctave broadband THz pulses. As a large part of the spectral content of those pulses falls outside the narrow-band plasmonic absorption, it is much harder to achieve efficient pumping and therewith high carrier temperatures with those sources. A fraction of the FEL power (~2%) was split off to serve as probe beam and passed a mechanical delay stage to set the time delay between pump and probe pulse. Both beams were then focused at near-normal incidence onto the sample with an off-axis parabolic mirror to an approximate spot size of 0.7 mm. A small angle between the pump and probe allowed the transmitted probe to be spatially separated and recorded using a Si bolometer as a function of the time delay between pump and probe pulse. A more detailed description, including a sketch of the setup, can be found in ref.[23] In order to observe the dynamical resonance shift, pump−probe measurements were conducted at six different frequencies chosen to be below and above the plasmon resonance, indicated by the vertical lines in Figure 2: 2.0, 2.5, 3.1, 3.9, 4.4, and 4.9 THz. To maximize the carrier cooling time and therewith the pump−probe signals,[10] the sample was held in a helium cryostat at a lattice temperature of 15 K throughout the measurements.

The strongest pump-induced transient is observed when the photon frequency is resonant with the plasmon frequency at 3.9 THz, and both pump and probe are copolarized perpendicular to the graphene ribbons. In this case, we observe a pump-induced increase in the transmission, as shown in Figure 3a. The highest measured change was 9%, which was

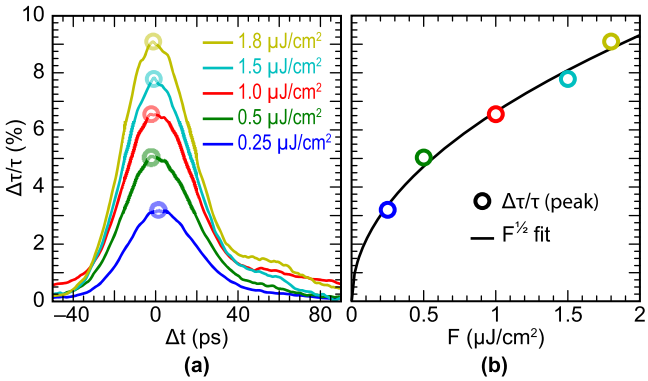

Figure 3. (a) Pump-induced change in THz transmission, measured at the plasmon resonance of 3.9 THz, for a variety of pump fluences. (b) Peak change in transmission as a function of the pump fluence, showing approximate square-root dependence (line).

observed at a fluence of 1.8 μJ cm^{-2}. The observed change in transmission increases with the pump fluence approximately in proportion to $F^{1/2}$, as shown in Figure 3b. We note that typical nonlinear effects scale quadratically or cubically with intensity. For the plasmonic nonlinearity the change in transmission scales with the square root of the intensity and it is already strong at comparably low fluence. Transmission changes of more than 5% are achieved at fluences of only 0.5 μJ cm^{-2}.

For the nonlinear measurements presented in Figure 3, both the pump and the probe are simultaneously resonant with the structure, which yields a compounded nonlinear enhancement: not only is the pump absorption resonantly increased, thereby leading to the strongest possible carrier heating, but the probe pulse is also tuned to the resonance, and is therefore very sensitive to induced changes in the plasmon frequency or linewidth. To better resolve the nature of the plasmonic nonlinearity, additional measurements were conducted at frequencies below and above the plasmon resonance, indicated by the vertical lines in Figure 2. For these measurements, the pump polarization was adjusted to be parallel to the graphene ribbons, a condition that excludes the resonant excitation of plasmons. Under these conditions, the pump pulse with a fluence of 1.5 μJ cm^2 heats the free carriers in the graphene through conventional Drude absorption, which only weakly depends on frequency over the spectral range considered. The probe polarization, meanwhile, was maintained perpendicular to the ribbons, thereby probing the plasmon resonance.

Figure 4a shows the observed pump−probe response at the six frequencies considered. Because the pump is no longer

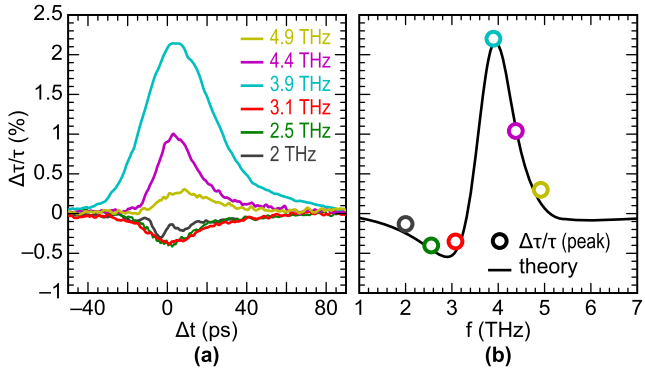

Figure 4. (a) Change in probe transmission through the sample measured at frequencies above and below the plasmon resonance for the case when the pump polarization is polarized parallel to the graphene ribbons, while the probe is polarized perpendicular. (b) Peak change in transmission as a function of the frequency. The crosses indicate the measurements presented in (a); the line is the result of the theoretical calculation based on a thermal model of hot electrons.

resonant with the structure, the peak change in transmission is smaller than in Figure 3. For frequencies below the resonance (2, 2.5, and 3.1 THz), the pump-induced change in transmission is negative, while for frequencies at or above the resonance (3.9, 4.4, and 4.9 THz), the response is positive, with the largest increase observed at the resonant frequency. As explained below, the change in sign can be explained by a pump-induced red-shift of the plasmon frequency.

3. THEORY AND ANALYSIS

For the probe signal, which is polarized perpendicular to the ribbons, the transmission spectrum $\tau(\omega)$ can be well approximated using a Drude-Lorentz model of the conductivity,[23]

$$\frac{\tau(\omega)}{\tau_0} = \left| 1 + \frac{wZ_0}{\pi\Lambda(1+n_{SiC})} \frac{D}{\left(\Gamma - i\frac{\omega^2-\omega_P^2}{\omega}\right)} \right|^{-2} \quad (1)$$

where w/Λ is the duty cycle of the graphene grating, Z_0 $(=\sqrt{\mu_0/\epsilon_0})$ is the vacuum impedance, and n_{SiC} is the substrate refractive index. The plasmon resonance frequency, linewidth, and strength are described by ω_P, Γ, and D, respectively. As

DOI: 10.1021/acsphotonics.8b01499
ACS Photonics 2019, 6, 302−307

illustrated by the dashed theory curve in Figure 2, this model accurately predicts the observed transmission spectrum for the graphene ribbons considered here. Equation 1 is plotted in Figure 5a, which shows specifically how the linewidth, resonance frequency, and strength are related to the transmission spectrum.

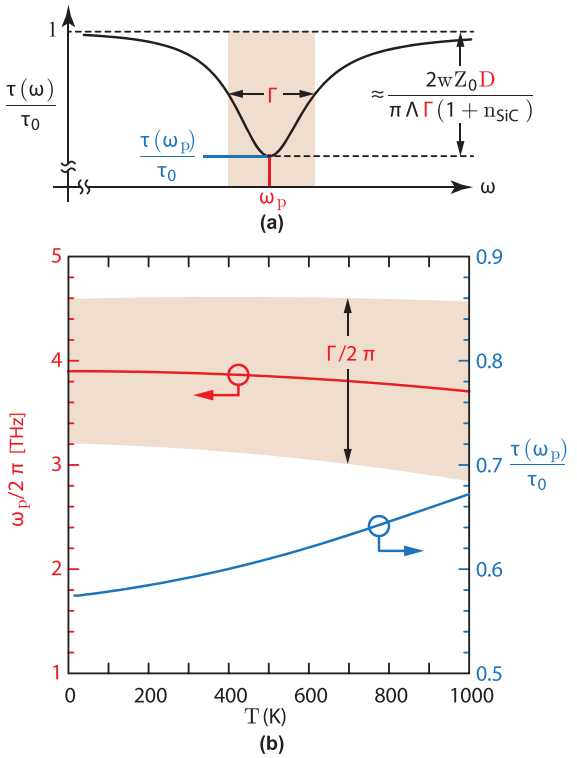

Figure 5. (a) Transmission spectrum for graphene ribbons (eq 1), normalized relative to that of a substrate with no graphene, obtained from the Drude Lorentz model of conductivity. The center frequency, width, and depth are related to the plasmon frequency ω_p, scattering rate Γ, and Drude weight D, respectively. These three parameters, indicated in red, are predicted to vary with the electron temperature T, as shown in (b).

The nonlinear response of the graphene ribbons can be explained by a two-temperature model, in which the optically excited carriers are heated to transient temperature T that exceeds the lattice temperature T_L. Because the electron−electron scattering time (approximately 10 fs in graphene) is much faster than the optical pulsewidths employed here, the optically excited carriers can be well characterized by a thermal distribution of hot carriers. All three of the Drude-Lorentz parameters appearing in eq 1 implicitly depend on the transient electron temperature T, according to

$$D(T) \simeq D_0\left(1 - \frac{\pi^2 k_B^2 T^2}{6\varepsilon_F^2}\right) \tag{2}$$

$$\omega_p(T) \simeq \omega_{p0}\left(1 - \frac{\pi^2 k_B^2 T^2}{12\varepsilon_F^2}\right) \tag{3}$$

$$\Gamma(T) \simeq \Gamma_0\left(1 + \frac{\pi^2 k_B^2 T^2}{6\varepsilon_F^2}\right) + \gamma T \tag{4}$$

The Drude weight, plasmon frequency, and scattering rate scale with the chemical potential as μ, $\mu^{1/2}$, and μ^{-1}, respectively, and the leading terms appearing in eqs 2−4 all arise from the temperature dependence of the chemical potential, which is expanded to second-order in k_BT/ε_F. The additional term appearing in eq 4 describes a temperature-dependent increase in the LA phonon scattering rate. The factor γ appearing in this equation is proportional to the acoustic deformation potential, and is equal to 1.264×10^{-3} K^{-1} ps^{-1} for the graphene considered here, as summarized in Table 1.

Table 1. Summary of Numerical, Physical, Geometrical, and Experimental Parameters and Conditions[a]

ε_F	Fermi energy	350 meV
$n = \frac{1}{\pi}\left(\frac{\varepsilon_F}{\hbar v_F}\right)^2$	carrier concentration	9.0×10^{12} cm^{-2}
$\mu_c = \frac{ev_F}{\sqrt{\pi n}\Gamma_0\hbar}$	carrier mobility	3600 cm^2 V^{-1} s^{-1}
w	graphene ribbon width	900 nm
Λ	graphene grating period	1200 nm
n_{SiC}	SiC substrate refractive index	3.5
$D_0 = \sqrt{\pi n}\, e^2 v_F/\hbar$	Drude weight	0.13 Ω^{-1} ps^{-1}
ω_{p0}	plasmon frequency	$2\pi\cdot$(3.9 THz)
$\Gamma_0 = \frac{ev_F}{\sqrt{\pi n}\mu_c\hbar}$	plasmon linewidth	8.7 ps^{-1}
T_L	lattice temperature	15 K
l	disorder mean free path	3 nm
$\alpha = 2\pi k_B^2\varepsilon_F/(3\hbar^2 v_F^2)$	specific heat	2.01×10^{-9} Jm^{2-} K^{-2}
$\beta = \zeta(3)V_D^2\varepsilon_F k_B^3/(\pi^2\rho\hbar^4 v_F^3 s^2 l)$	supercollision cooling coefficient	0.37 Wm^{2-} K^{-3}
$\gamma = \frac{k_B V_D^2\varepsilon_F}{4\hbar^3 v_F^2\rho s^2}$	LA phonon scattering coefficient	1.26×10^{-3} K^{-1} ps^{-1}

[a]The expressions given here use the following accepted physical constants for graphene: $v_F = 10^6$ ms^{-1} represents the Fermi velocity, $V_D = 10$ eV is the acoustic deformation potential, $\rho = 7.6 \times 10^{-7}$ kg m^{-2} is the density, and $s = 2.1 \times 10^4$ ms^{-1} is the acoustic velocity.

Taken together, eqs 2−4 predict that when the electron temperature increases under THz illumination, the plasmon resonance will weaken, broaden, and red-shift to lower frequencies. Figure 5b plots how the Drude weight, linewidth and plasmon frequency vary with the electron temperature. Figure 6a plots the calculated transmission spectrum for electron temperatures up to 1000 K, calculated for the graphene conditions considered here, clearly showing this effect. The thermally induced red shift causes the transmission to decrease for frequencies below the resonance, but increase above resonance, in agreement with the measurements presented in Figure 4.

To model the temporal evolution of the pump-induced change in transmission, we numerically solved the nonlinear thermal equation[32]

$$\alpha T\frac{dT}{dt} + \beta(T^3 - T_L^3) = A(\omega, T)I(t) \tag{5}$$

DOI: 10.1021/acsphotonics.8b01499
ACS Photonics 2019, 6, 302−307

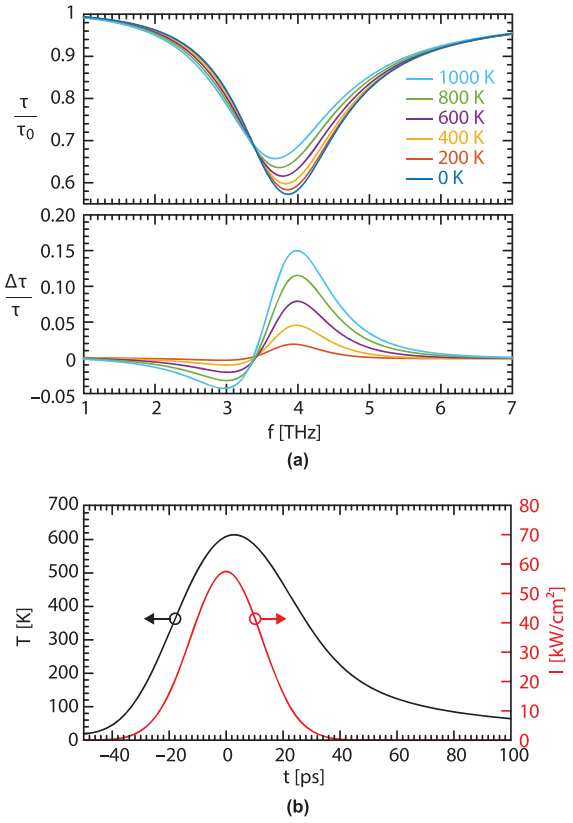

Figure 6. (a) Upper: Calculated normalized transmission for electron temperatures up to 1000 K, showing the predicted red-shift of the plasmon when the electrons are heated. Lower: Corresponding fractional change in transmission $\Delta\tau/\tau$. (b) Calculated transient electron temperature as a function of time, together with the incident pulse intensity $I(t)$, for a 1.8 μJ cm^{-2} Gaussian pulse of 29 ps duration (fwhm), for which the peak electron temperature reaches 610 K.

where αT is the specific heat of graphene, β describes the disorder-assisted cooling coefficient of hot carriers,[32,33] $A(\omega,T)$ is the power absorption coefficient in the graphene film, and $I(t)$ is the incident pump intensity, which in these experiments describes a Gaussian pulse with a full width at half-maximum (FWHM) of 29 ps. As summarized in Table 1, the two parameters α and β appearing in eq 5 are entirely determined by the Fermi energy and mean free path (which characterizes the level of disorder in the sample.)

The time scale for hot-carrier cooling can be estimated by setting the right-hand side of eq 5 to zero, and assuming $T \gg T_L$, in which case eq 5 may be directly integrated to find

$$T(t) = \frac{T_0}{1 + \frac{\beta T_0}{\alpha} t} \tag{6}$$

where T_0 represents the peak (initial) electron temperature produced by the pump pulse. If we assume a peak temperature of T_0 = 610 K (the maximum level predicted for the experimental conditions considered here), the electrons will cool to half their initial temperature over a time of $\alpha/\beta T_0$ = 8.8 ps. Although the relationship between temperature and transmission is nonlinear, the time scale estimated here is consistent with the response time observed in the pump–probe measurements in Figure 4a.

Figure 6b plots the calculated electron temperature, obtained by solving eq 5, together with the incident pulse intensity $I(t)$, for a 1.8 μJ cm^{-2} Gaussian pulse of 29 ps duration, for which the peak electron temperature is predicted to reach 610 K.

Figure 4b plots the peak differential change in transmission as a function of frequency for the five frequencies considered here. The solid line indicates the result predicted by numerically calculating the electron temperature $T(t)$ (eq 5) and using eqs 1–4 to determine the consequent change in transmission. The experimental observations are in excellent agreement with the theoretical predictions and clearly show evidence of the transient red-shift in the plasmon frequency.

The theoretical model used exclusively the parameters taken or inferred from separately conducted measurements: the carrier concentration and plasmon linewidth were inferred from linear FTIR transmission measurements of patterned and unpatterned graphene in Figure 2. The cooling coefficient β (and consequently the disorder mean-free path l) was chosen to match the power dependence in Figure 3b. All of the remaining model parameters are derived from these, using well-defined relationships and accepted physical constants for graphene, as summarized in Table 1. The only adjustable parameter needed to match the data shown in Figure 4b was that the absorbed pump power was reduced by a factor of approximately two relative to what was assumed in the copolarized case. We believe that this discrepancy could be explained by the (unmeasured) difference in spatial overlap between the pump and the probe between the two measurements, although we acknowledge that this could also be evidence of anisotropic thermal distribution of carriers.

The wavelength dependence of the nonlinear absorption allows employing graphene ribbons either as a saturable absorber or saturable transmitter. The low heat capacity of the charge carriers in the graphene leads to a pronounced increase of the carrier temperature, even when excited at moderate fluence that is achievable with table-top sources. As the plasmon frequency of the ribbons can be tuned, either by changing the ribbon dimensions or by gating, graphene ribbons can feature a strong nonlinearity in a wide spectral range from THz to mid-infrared radiation. Even stronger nonlinearity is expected if higher quality graphene is used or if additional longitudinal enhancement is introduced through a resonant cavity. As the carrier phonon cooling in graphene is very efficient, the pump-induced change in transmission is mostly limited to the duration of the pump pulse, which is consistent with pump–probe experiments on unpatterned graphene in this wavelength range. This makes the thermal nonlinearity in graphene ribbons suitable for ultrafast processes.

4. CONCLUSION

Graphene plasmons provide a platform for nonlinear THz materials that can be tailored to a desired wavelength. The low specific heat of the carriers in graphene, in combination with a fast thermal relaxation, leads to strong nonlinearities with a short lifetime of about 9 ps, even at moderate fluence that is achievable with table-top laser sources. As the resonance frequency changes with temperature, an array of graphene ribbons can serve either as a saturable absorber or saturable transmitter, depending on whether the photon frequency is below or at/above resonance, respectively. Adding up several layers of ribbons, the nonlinearity can be further enhanced.

DOI: 10.1021/acsphotonics.8b01499
ACS Photonics 2019, 6, 302–307

AUTHOR INFORMATION

Corresponding Author

*E-mail: mj2838@columbia.edu.

ORCID

Thomas E. Murphy: 0000-0002-8286-3832

Martin Mittendorff: 0000-0003-3998-2518

Notes

The authors declare no competing financial interest.

ACKNOWLEDGMENTS

The sample fabrication was carried out at the University of Maryland Nanocenter. Support from P. Michel and the FELBE team is gratefully acknowledged. This work was supported by the Office of Naval Research (ONR; N000141310865) and National Science Foundation (NSF) (ECCS 1309750). Work at NRL was supported by ONR. We acknowledge financial support of the Deutsche Forschungsgemeinschaft through SFB 1242.

REFERENCES

(1) Breusing, M.; Kuehn, S.; Winzer, T.; Malić, E.; Milde, F.; Severin, N.; Rabe, J. P.; Ropers, C.; Knorr, A.; Elsaesser, T. Ultrafast nonequilibrium carrier dynamics in a single graphene layer. *Phys. Rev. B: Condens. Matter Mater. Phys.* **2011**, *83*, 153410.

(2) Dawlaty, J. M.; Shivaraman, S.; Chandrashekhar, M.; Rana, F.; Spencer, M. G. Measurement of ultrafast carrier dynamics in epitaxial graphene. *Appl. Phys. Lett.* **2008**, *92*, 042116.

(3) Obraztsov, P. A.; Rybin, M. G.; Tyurnina, A. V.; Garnov, S. V.; Obraztsova, E. D.; Obraztsov, A. N.; Svirko, Y. P. Broadband Light-Induced Absorbance Change in Multilayer Graphene. *Nano Lett.* **2011**, *11*, 1540−1545.

(4) Hong, S.-Y.; Dadap, J. I.; Petrone, N.; Yeh, P.-C.; Hone, J.; Osgood, R. M. Optical Third-Harmonic Generation in Graphene. *Phys. Rev. X* **2013**, *3*, 021014.

(5) Kumar, N.; Kumar, J.; Gerstenkorn, C.; Wang, R.; Chiu, H.-Y.; Smirl, A. L.; Zhao, H. Third harmonic generation in graphene and few-layer graphite films. *Phys. Rev. B: Condens. Matter Mater. Phys.* **2013**, *87*, 121406.

(6) Hendry, E.; Hale, P. J.; Moger, J.; Savchenko, A. K.; Mikhailov, S. A. Coherent Nonlinear Optical Response of Graphene. *Phys. Rev. Lett.* **2010**, *105*, 097401.

(7) Gu, T.; Petrone, N.; McMillan, J. F.; van der Zande, A.; Yu, M.; Lo, G. Q.; Kwong, D. L.; Hone, J.; Wong, C. W. Regenerative oscillation and four-wave mixing in graphene optoelectronics. *Nat. Photonics* **2012**, *6*, 554−559.

(8) Bao, Q.; Zhang, H.; Wang, Y.; Ni, Z.; Yan, Y.; Shen, Z. X.; Loh, K. P.; Tang, D. Y. Atomic-Layer Graphene as a Saturable Absorber for Ultrafast Pulsed Lasers. *Adv. Funct. Mater.* **2009**, *19*, 3077−3083.

(9) Zhang, H.; Tang, D. Y.; Zhao, L. M.; Bao, Q. L.; Loh, K. P. Large energy mode locking of an erbium-doped fiber laser with atomic layer graphene. *Opt. Express* **2009**, *17*, 17630−17635.

(10) Winnerl, S.; Orlita, M.; Plochocka, P.; Kossacki, P.; Potemski, M.; Winzer, T.; Malic, E.; Knorr, A.; Sprinkle, M.; Berger, C.; de Heer, W. A.; Schneider, H.; Helm, M. Carrier Relaxation in Epitaxial Graphene Photoexcited Near the Dirac Point. *Phys. Rev. Lett.* **2011**, *107*, 237401.

(11) Hwang, H. Y.; Brandt, N. C.; Farhat, H.; Hsu, A. L.; Kong, J.; Nelson, K. A. Nonlinear THz Conductivity Dynamics in P-Type CVD-Grown Graphene. *J. Phys. Chem. B* **2013**, *117*, 15819−15824.

(12) Jnawali, G.; Rao, Y.; Yan, H.; Heinz, T. F. Observation of a Transient Decrease in Terahertz Conductivity of Single-Layer Graphene Induced by Ultrafast Optical Excitation. *Nano Lett.* **2013**, *13*, 524−530.

(13) Mics, Z.; Tielrooij, K.-J.; Parvez, K.; Jensen, S. A.; Ivanov, I.; Feng, X.; Müllen, K.; Bonn, M.; Turchinovich, D. Thermodynamic picture of ultrafast charge transport in graphene. *Nat. Commun.* **2015**, *6*, 7655.

(14) Hafez, H. A.; et al. Extremely efficient terahertz high-harmonic generation in graphene by hot Dirac fermions. *Nature* **2018**, *561*, 507−511.

(15) Atwater, H. A.; Polman, A. Plasmonics for improved photovoltaic devices. *Nat. Mater.* **2010**, *9*, 205−213.

(16) Kauranen, M.; Zayats, A. V. Nonlinear Plasmonics. *Nat. Photonics* **2012**, *6*, 737−748.

(17) Ju, L.; Geng, B.; Horng, J.; Girit, C.; Martin, M.; Hao, Z.; Bechtel, H. A.; Liang, X.; Zettl, A.; Shen, Y. R.; Wang, F. Graphene plasmonics for tunable terahertz metamaterials. *Nat. Nanotechnol.* **2011**, *6*, 630−634.

(18) Low, T.; Avouris, P. Graphene Plasmonics for Terahertz to Mid-Infrared Applications. *ACS Nano* **2014**, *8*, 1086−1101.

(19) Koppens, F. H. L.; Chang, D. E.; García de Abajo, F. J. Graphene Plasmonics: A Platform for Strong Light-Matter Interactions. *Nano Lett.* **2011**, *11*, 3370−3377.

(20) Gullans, M.; Chang, D. E.; Koppens, F. H. L.; de Abajo, F. J. G.; Lukin, M. D. Single-Photon Nonlinear Optics with Graphene Plasmons. *Phys. Rev. Lett.* **2013**, *111*, 247401.

(21) Grigorenko, A. N.; Polini, M.; Novoselov, K. S. Graphene plasmonics. *Nat. Photonics* **2012**, *6*, 749−758.

(22) Hu, F.; Luan, Y.; Fei, Z.; Palubski, I. Z.; Goldflam, M. D.; Dai, S.; Wu, J.-S.; Post, K. W.; Janssen, G. C. A. M.; Fogler, M. M.; Basov, D. N. Imaging the Localized Plasmon Resonance Modes in Graphene Nanoribbons. *Nano Lett.* **2017**, *17*, 5423−5428.

(23) Jadidi, M. M.; König-Otto, J. C.; Winnerl, S.; Sushkov, A. B.; Drew, H. D.; Murphy, T. E.; Mittendorff, M. Nonlinear Terahertz Absorption of Graphene Plasmons. *Nano Lett.* **2016**, *16*, 2734−2738.

(24) Cox, J. D.; de Abajo, F. J. G. Transient nonlinear plasmonics in nanostructured graphene. *Optica* **2018**, *5*, 429−433.

(25) Riedl, C.; Coletti, C.; Starke, U. Structural and electronic properties of epitaxial graphene on SiC (0001): a review of growth, characterization, transfer doping and hydrogen intercalation. *J. Phys. D: Appl. Phys.* **2010**, *43*, 374009.

(26) Emery, J. D.; Wheeler, V. D.; Johns, J. E.; McBriarty, M. E.; Detlefs, B.; Hersam, M. C.; Kurt Gaskill, D.; Bedzyk, M. J. Structural consequences of hydrogen intercalation of epitaxial graphene on SiC(0001). *Appl. Phys. Lett.* **2014**, *105*, 161602.

(27) Daniels, K. M.; Jadidi, M. M.; Sushkov, A. B.; Nath, A.; Boyd, A. K.; Sridhara, K.; Drew, H. D.; Murphy, T. E.; Myers-Ward, R. L.; Gaskill, D. K. Narrow plasmon resonances enabled by quasi-freestanding bilayer epitaxial graphene. *2D Mater.* **2017**, *4*, 025034.

(28) Avouris, P.; Dimitrakopoulos, C. Graphene: synthesis and applications. *Mater. Today* **2012**, *15*, 86−97.

(29) Speck, F.; Jobst, J.; Fromm, F.; Ostler, M.; Waldmann, D.; Hundhausen, M.; Weber, H. B.; Seyller, T. The quasi-free-standing nature of graphene on H-saturated SiC(0001). *Appl. Phys. Lett.* **2011**, *99*, 122106.

(30) Tedesco, J. L.; VanMil, B. L.; Myers-Ward, R. L.; McCrate, J. M.; Kitt, S. A.; Campbell, P. M.; Jernigan, G. G.; Culbertson, J. C.; Eddy, C. R.; Gaskill, D. K. Hall effect mobility of epitaxial graphene grown on silicon carbide. *Appl. Phys. Lett.* **2009**, *95*, 122102.

(31) Jadidi, M. M.; Sushkov, A. B.; Myers-Ward, R. L.; Boyd, A. K.; Daniels, K. M.; Gaskill, D. K.; Fuhrer, M. S.; Drew, H. D.; Murphy, T. E. Tunable Terahertz Hybrid Metal-Graphene Plasmons. *Nano Lett.* **2015**, *15*, 7099−7104.

(32) Song, J. C. W.; Reizer, M. Y.; Levitov, L. S. Disorder-Assisted Electron-Phonon Scattering and Cooling Pathways in Graphene. *Phys. Rev. Lett.* **2012**, *109*, 106602.

(33) Viljas, J. K.; Heikkilä, T. T. Electron-phonon heat transfer in monolayer and bilayer graphene. *Phys. Rev. B: Condens. Matter Mater. Phys.* **2010**, *81*, 245404.

DOI: 10.1021/acsphotonics.8b01499
ACS Photonics 2019, 6, 302−307